ACI STRUCTURAL JOURNAL TECHNICAL PAPER

Title No. 117-S81

Shear Behavior of Thick Slabs

by Michael P. Collins, Phillip T. Quach, and Evan C. Bentz

Thick reinforced concrete members not containing shear reinforcement can fail at shear stresses significantly lower than those specified by the 2014 ACI Code. This is because the traditional ACI shear provisions were based on tests of small specimens, and do not account for the size effect in shear. This paper focuses on an experimental program in which a 4000 mm (13 ft) thick slab strip specimen and a 300 mm (12 in.) deep companion specimen were constructed and tested to failure. These tests extend the range of a series of 17 such slab strip experiments previously tested at the University of Toronto. The results show that the 2014 ACI Code can give dangerously high estimates of shear capacity for very thick slabs not containing shear reinforcement. The research also shows that minimum shear reinforcement greatly increases both the strength and deformability of thick slabs.

Keywords: aggregate interlock; cracking; design equations; safety; shear; size effect; stirrups; test/experiment; thick slabs.

INTRODUCTION

Modern infrastructure often incorporates very thick reinforced concrete members that are critical elements in the load-carrying system of the structure. Transfer slabs, footings, and mat foundations in high-rise construction are examples of such members. As building heights increase, demands on these members generally become greater, resulting in larger member depths. Thus, the 73-story-tall Wilshire Grand Center in Los Angeles, CA, has a 5.4 m (17 ft, 9 in.) thick mat foundation.[1] Refer to Fig. 1.

For construction efficiency, mat foundations are traditionally designed to be thick enough to avoid the need for shear reinforcement. However, thick slabs without shear reinforcement are susceptible to premature shear failure. Experimental research and analytical models have shown that the shear stress to cause shear failure of members without shear reinforcement decreases as the depth of the member increases, a phenomenon known as the size effect in shear.[2-5] Because many international codes, including the 2014 ACI Code,[6] do not appropriately account for this size effect, it is possible to have a range of predicted shear strengths for a given thick slab which can vary[7] by factors of up to three depending upon which codes are being compared.[8] These major disagreements in predicted shear strength contrast strongly with the situation for flexural strength, where all major international codes give almost identical predictions.

The 2014 ACI shear provisions, essentially the same as those of the 1963 then-new provisions, based on 10 years of extensive research and a large database of available tests, were adopted. Unfortunately, the specimens in the database had an average effective depth of only 340 mm (13 in.)[5] and even today,[9] relatively few large shear specimens have been tested, with only 10% of shear tests having an effective depth greater than 610 mm (24 in.) and only 4% greater than

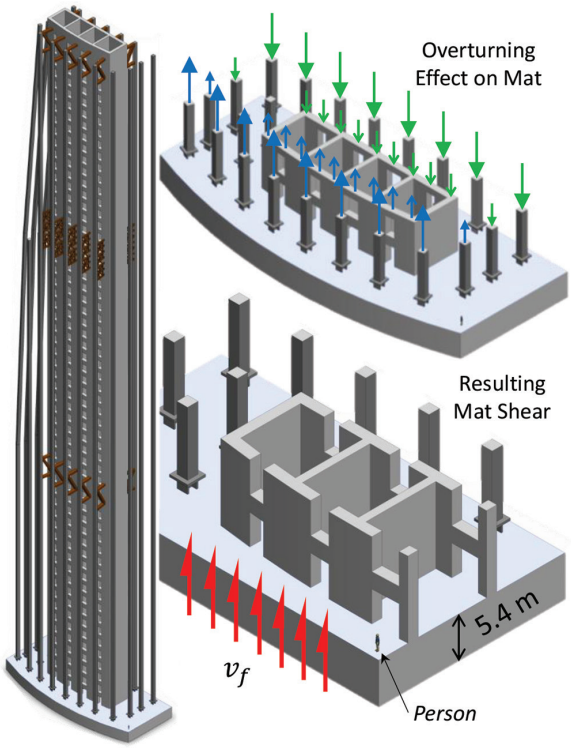

Fig. 1—Schematic of Wilshire Grand mat foundation resisting overturning effects from lateral loads.

1000 mm (39 in.). Prior to the specimen discussed in this paper, the largest shear test was from Japan,[4] had a depth of 3 m (10 ft), was uniformly loaded, and had significant longitudinal bar cutoffs.

This paper discusses the construction, loading to failure, and detailed measured behavior of a specimen with an overall depth of 4 m (13 ft, 1 in.). In addition, a companion specimen with a more traditional specimen depth of 300 mm (12 in.) was cast using the same concrete. These two specimens represent strips "cut" from one-way slabs. The experiments were designed to extend the range of size effect shear experiments previously conducted at the University of Toronto to a scale more representative of the large structural members in use today. As an effective means of mitigating the size effect in thick slab-type elements is to provide minimum shear reinforcement, the very thick slab strip contained stirrups in one of the two shear spans to assess the beneficial effects of such reinforcement.

ACI Structural Journal, V. 117, No. 4, July 2020.
MS No. S-2019-201, doi: 10.14359/51724666, received May 17, 2019, and reviewed under Institute publication policies. Copyright © 2020, American Concrete Institute. All rights reserved, including the making of copies unless permission is obtained from the copyright proprietors. Pertinent discussion including author's closure, if any, will be published ten months from this journal's date if the discussion is received within four months of the paper's print publication.

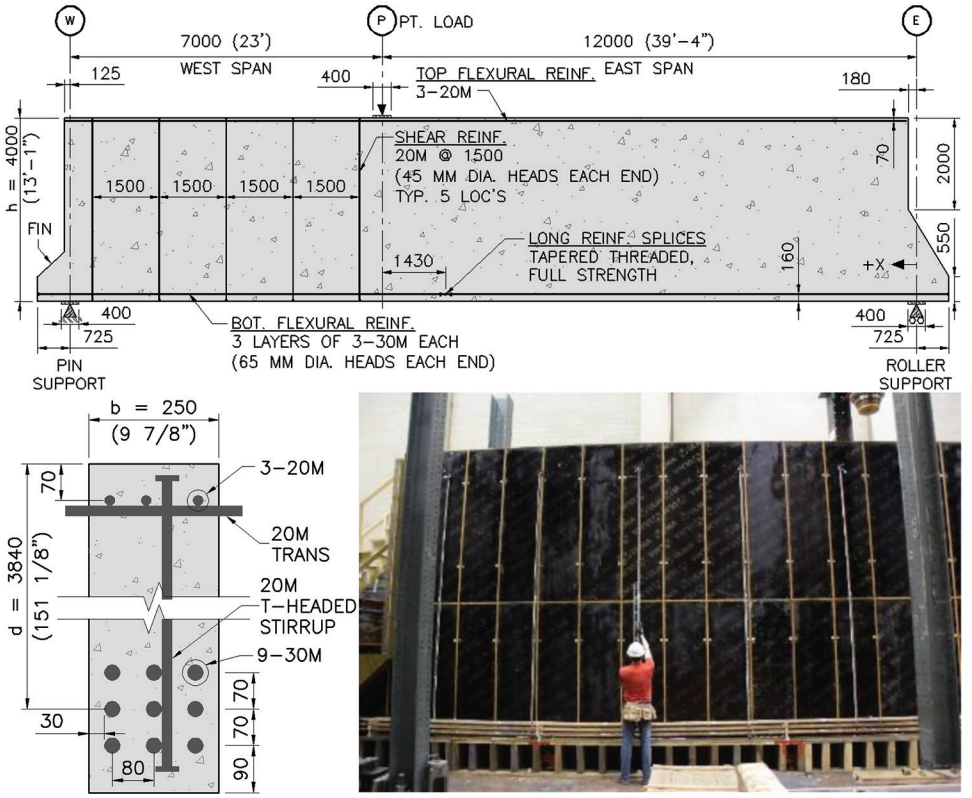

Fig. 2—PLS4000 specimen details: dimensions in mm. (Note: 1 mm = 0.04 in.)

Prior to testing the large specimen, a prediction competition was held to evaluate how academics and practicing engineers would fare in estimating the shear response. A comparison of the predictions provided by the 66 entries with the preliminary results of the experiments has been given in a previous ACI publication.[8] An important observation from the competition is that half of these experienced engineers submitted predictions from 1.5 to 5.5 times higher than the actual failure load.

The primary purpose of this paper is to provide definitive documentation of the new large slab strip experiments. It will offer detailed data about the mechanism of shear failure in such large reinforced concrete members. The three new experimental results will be compared with 17 similar size effect experiments that have been constructed using the same concrete supplier and tested in the same laboratory. The results demonstrate that the size effect is predictable and that the very beneficial effects on shear strength and deformability of thick slabs that can be achieved by adding just a minimum quantity of shear reinforcement are also predictable.

RESEARCH SIGNIFICANCE

The research summarized in this paper demonstrates that the 2014 ACI shear provisions, which neglect the size effect in shear, are unsafe. Adding just a minimum quantity of shear reinforcement is shown to suppress this detrimental size effect.

EXPERIMENTAL PROGRAM

Design of specimens

The details of Specimen PLS4000 are shown in Fig. 2. The specimen, which is a simply supported beam with a span of 19.0 m (62 ft, 4 in.), represents a 250 mm (9.8 in.) wide strip cut from a 4 m (13 ft, 1 in.) thick one-way slab. PLS4000 was designed to obtain two tests from the single large specimen. The simple span was divided at the location of the displacement-controlled actuator into a 12 m (39 ft, 4 in.) long east shear span containing no shear reinforcement and a 7 m (23 ft) long west shear span containing the ACI specified minimum amount of shear reinforcement. The weaker east shear span, PLS4000E, was designed to fail first, and then after strengthening the failed east shear span with external post-tensioned vertical bars, the west shear span, PLS4000W, would be loaded to failure.

The flexural tension reinforcement consisted of nine 30M bars (A_s = 6300 mm^2 [9.76 in.^{2}]). To facilitate transportation of these bars and specimen construction, they were coupled with tapered threaded mechanical splices able to achieve the full strength of the bars. The bars also had 65 mm (2.6 in.) diameter steel heads welded to each end to ensure full development. The "fins" at each end of the specimen provided a region for the longitudinal bars to develop and also resist local stress concentrations in the vicinity of the heads. The effective depth d of this reinforcement was 3840 mm (151.2 in.).

Transverse shear reinforcement in the west shear span consisted of single leg 20M bars (A_s = 300 mm^2 [0.465 in.^{2}]) with 45 mm (1.8 in.) diameter heads welded on each end. The single leg bars were spaced at 1500 mm (59 in.), resulting in

Fig. 3—Loading and lateral bracing of PLS4000.

a total of five bars within the shear span. The stirrup spacing, 0.39*d*, satisfies the ACI stirrup spacing limit of 0.5*d*, but exceeds the maximum spacing limit of 610 mm (24 in.).

Specimen PLS4000 contained 19.4 m^3 (25.6 yd^3) of concrete, which took three concrete trucks to cast. Trucks 1, 2, and 3 provided 37.5%, 37.5%, and 25% of the concrete, respectively. The concrete and the 1200 kg (2650 lb) of reinforcing steel resulted in a specimen weighing 48 tonnes (53 tons).

The more traditional size specimen, PLS300, had an overall depth of 300 mm (11.8 in.), a width of 175 mm (6.9 in.), two equal shear spans of 825 mm (32.5 in.), and an overall length of 1800 mm (71 in.). The flexural tension reinforcement consisted of three 10M bars (A_s = 3 × 100 = 300 mm^2 [0.465 $in.^2$]) at an effective depth *d* of 264 mm (10.4 in.). The loading plate and the bearing plates were all 38 mm (1.5 in.) wide, which is approximately 10 times smaller than the plates used for PLS4000 (refer to Fig. 2). PLS300 was cast using concrete from Truck 1 and weighed 227 kg (500 lb). Thus, PLS4000 was 210 times heavier than PLS300.

Loading apparatus and test protocol

To provide restraint against lateral-torsional buckling, moment-resisting frames (MRF) were placed near each of the two end supports and at the loading location. Each MRF supported four low-friction lateral restraints—two on the north face of the specimen and two on the south—that were in contact with the concrete to prevent out-of-plane

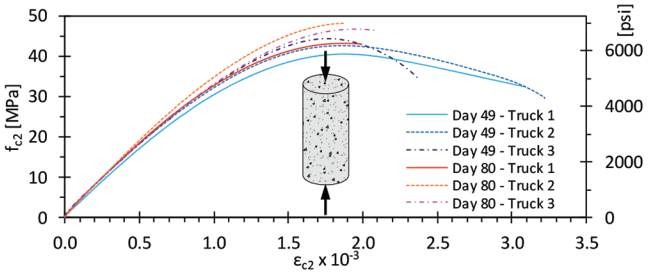

Age, Days	f_c', MPa	ε'_c, $\times 10^{-3}$	E_c, MPa
49	43.2	1.89	34,400
80	45.3	1.91	36,300

(a) Concrete stress-strain curves

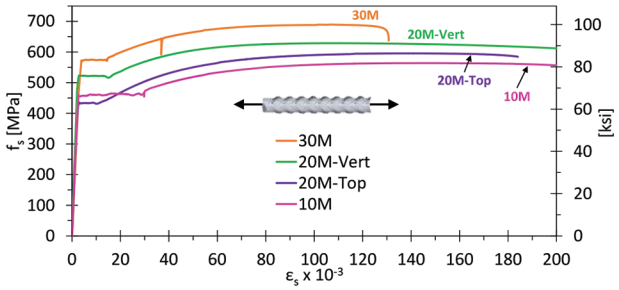

Bar	A_b, mm^2	f_y, MPa	f_u, MPa	E_s, MPa	ε_{sh}, $\times 10^{-3}$	ε_u, $\times 10^{-3}$
30M	700	573	688	190,500	13.4	96
20M Top	300	434	596	196,000	11.9	144
20M Vert.	300	522	629	228,100	16.7	112
10M	100	458	564	185,400	28.0	148

(b) Reinforcement stress-strain curves

Fig. 4—Material properties.

movement. The frame located at the load location was stiffened by an outrigger brace anchored into the strong floor; refer to Fig. 3.

Loading of PLS4000 was done in three-point bending with an off-center point load, *P*, located at gridline *P* shown in Fig. 2. The load was monotonically applied in displacement-control, Δ, using a hydraulic jack controlled by a servo-valve.

Material properties

Concrete used in the test specimens had a specified 28-day compressive strength of 30 MPa (4350 psi) and a maximum aggregate size (crushed limestone) of 14 mm (0.55 in.). A total of 44 cylinders, 150 x 300 mm (6 x 12 in.), were tested to monitor the concrete strengths from the three trucks in the period from 7 days until 100 days after casting. The concrete stress-strain responses measured on day 49 and day 80 after casting are shown in Fig. 4(a). It can be seen that at 49 days, when Specimen PLS4000E failed, the weighted average of the concrete strengths from the three trucks was 43.2 MPa (6260 psi), with the highest-strength Truck 3 being 8% stronger than lowest-strength Truck 1.

Specimen PLS4000W was failed 63 days after casting of the concrete and based on the 49- and 80-day strengths shown in Fig. 4, the concrete strength at this time can be interpolated to be 44.2 MPa (6410 psi). Specimen PLS300 was cast just from Truck 1 and was tested to failure at 99 days after casting, at which time the concrete strength was 44.8 MPa (6500 psi).

The stress-strain characteristics of the four different types of reinforcing bars used in PLS4000 and PLS300 are summarized in Fig. 4(b).

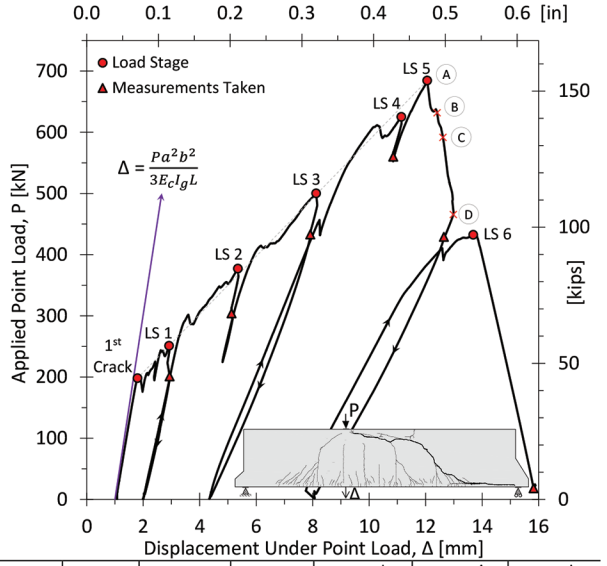

Load Stage	P, kN	P_{meas}, kN	Δ, mm	w_{max}*, mm	x_{crack}†, m	ε_{long}‡, x 10^{-3}
Crack	198	-	1.80	-	-	0.03
1	251	201	2.92	0.25	10.5	0.38
2	377	304	5.35	0.35	7.5	0.46
3	500	433	8.12	0.45	6.5	0.75
4	625	560	11.1	0.90	6.0	0.89
5	685	429	12.1	4.5	4.0	0.94
6	433	13	13.7	35	3.5	0.72

* Max crack width in east span
† Location of eastern-most crack
‡ Maximum measured longitudinal reinforcement strain

Fig. 5—Load-deformation response of PLS4000E.

Instrumentation

The instrumentation included load cells, reinforcement strain gauges, externally mounted linear variable differential transformers (LVDTs), and three-dimensional (3-D) coordinate measurements. More complete details of the instrumentation, the specimens, and the experiments can be found elsewhere.[10]

BEHAVIOR OF EAST SPAN WITHOUT SHEAR REINFORCEMENT

Load-deformation response

The load-deformation plot shown in Fig. 5 summarizes the response of PLS4000E and the key observations recorded during the six load stages (LS). Testing took 3 days from onset of loading to failure of the specimen at LS5, with an extra morning dedicated to reloading the damaged specimen, LS6. The initial deflection when P was 0 shown in Fig. 5 is the calculated self-weight deflection of the uncracked slab strip. First flexural cracking occurred when P was 198 kN (44.6 kip), indicating a flexural concrete tensile strength of 2.48 MPa (360 psi).[11] Between first cracking and ultimate load, the response of the slab strip follows a nearly linear path with an effective tangent stiffness only 19% of the stiffness prior to cracking. At load stages 1 through 4, the displacement of the jack was reduced until the applied load came down by approximately 15% to ensure the safety of the students and technicians involved in marking new cracks and measuring the widths of the cracks. The research of Calvi et al.[12] has shown that during such unloading, the crack widths and crack slips do not change significantly. In this paper, the highest load recorded will be labeled as P, while the load at which the measurements took place will be labeled as P_{meas}. The full recorded crack diagrams and widths at each load stage are presented in the Appendix (Fig. A1).

PLS4000E failed when P reached 685 kN (154 kip) with the propagation, opening, and slipping of a single large diagonal crack that initiated from a vertical flexural crack at 5.7 m (19 ft) from the east support. Figure 6 shows the crack widths and crack slips measured at LS5 along this failure crack and along a neighboring diagonal crack, which did not fail. The measured crack slips are underlined. For the diagonal crack which did not fail, initiating from the vertical crack at 8.5 m (28 ft), the crack widths were up to 1.0 mm

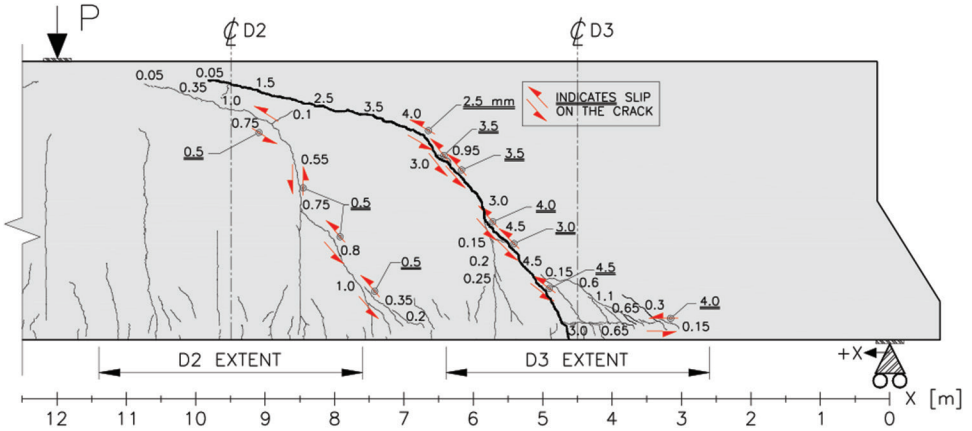

Fig. 6—PLS4000E crack widths and slips at LS5.

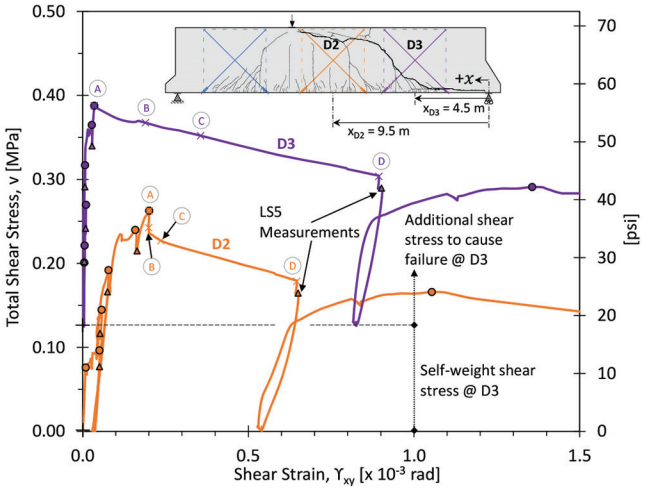

(a) Shear Stress - Shear Strain Response

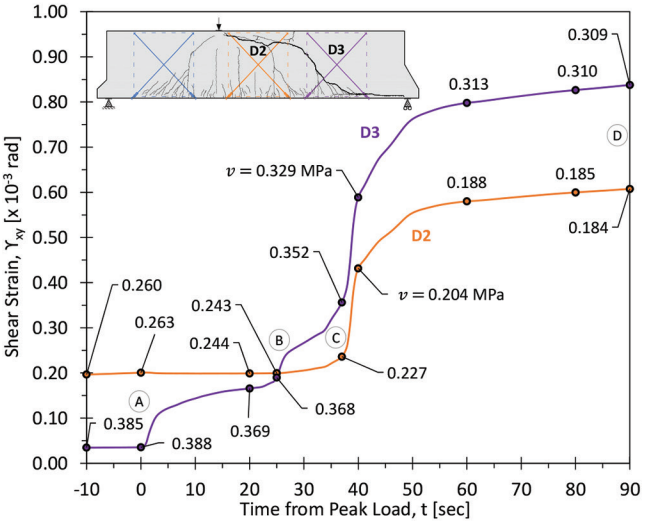

(b) History of Post-Peak Shear Strain Development

Fig. 7—PLS4000E development of failure mechanism.

(0.040 in.) wide and the ratios of slip-to-width were from 0.50 to 0.67. For the diagonal crack that failed, the crack widths were up to 4.5 mm (0.177 in.) and the slip-to-width ratios were from 0.63 to 1.33 with a measured average slip-to-average-width ratio of 0.92.

As the failure crack widened and the shear stress transmitted across this crack reduced, the "concrete tooth cantilever" between the two vertical cracks was bent to the left, causing vertical tensile stresses at the top right of this tooth. These tooth-bending tensile stresses caused the substantial change in the inclination of the diagonal failure crack that occurred as it reached the top of the "cantilever" and entered the flexural compression zone.

When the crack widths and slips had been measured at LS5, the specimen was unloaded for the weekend, after which the specimen was reloaded to assess its remaining capacity. At an applied point load P of 433 kN (97.4 kip), the major diagonal crack from LS5 significantly widened, and the actuator force simultaneously dropped down to 13 kN (2.9 kip). Crack widths at middepth of the main failure crack increased from 3 to 35 mm (0.12 to 1.38 in.).

Details of failure mechanism of PLS4000E

To discuss the sequence of events that led to the applied point load dropping by 32% from the peak load at LS5, as the imposed displacement increased by 7%, it is useful to identify stages A, B, C, and D in Fig. 5. A is at the peak load and D is 134 seconds after the peak load when the decision was taken to manually reduce the imposed displacement so the crack widths and crack slips could be safely measured.

Figures 7(a) and (b) show the measured shear stress-shear strain response for two regions, D2 and D3, of PLS4000E as measured by the four "full-depth" diagonal LVDTs covering two square regions each 3.8 x 3.8 m (12.5 x 12.5 ft); refer to inset in Fig. 7(a). For region D3, the average shear stress includes the shear at the center of the region due to self-weight of the slab strip. However, for D2, the center of the region is at midspan and hence the average self-weight shear for D2 is zero. From Fig. 7(a) it can be seen that in both regions the measured shear strains were nearly zero until flexural cracking occurred—first in D2 and then much later in D3, increased after cracking, and became significantly larger after the peak load was reached at Stage A. Figure 7(b) shows how these large post-peak shear strains evolved with time.

Between Stages A and B, a period of 25 seconds, there was a significant drop in the load required to deform the specimen, indicating the formation of the diagonal crack which ultimately caused the failure. Note that between A and B, there was a significant increase of shear strain in region D3 but a small elastic decrease of shear strain in region D2, indicating that the new diagonal crack had not yet propagated into region D2; refer to Fig. 7(a) and (b). At Stage B, a significant increase in the rate at which the shear strains in region D3 were increasing occurred. As a diagonal crack widens, its ability to transmit aggregate interlock stresses across the crack reduces (Walraven[13]) and significant crack slipping is required if the shear stress on the crack is to be maintained. The Modified Compression Field Theory (MCFT)[14,15] relates the magnitude of possible interface shear stress, v_{ci}, to the crack width w, the concrete strength f_c', and the maximum aggregate size a_g by Eq. (1), where the crack width and aggregate size are in mm and the concrete strength is in MPa. If psi and inch units are used, the 0.18 is replaced by 2.2 and the 16 is replaced by 0.63.

$$v_{ci} = \frac{0.18\sqrt{f_c'}}{0.31 + \frac{24w}{a_g + 16}} \quad (1)$$

At the section where failure initiated, 5.7 m (19 ft) from the east support, the highest shear force was 344 kN (77.4 kip), 27% of which was caused by the large self-weight of the specimen. The shear stress distribution across the depth of a cracked reinforced concrete member corresponds closely[16] to that proposed by Mörsch in the early 1900s and used by ACI codes until 1963. The shear stress transmitted across the crack is $V/(b_w jd)$, where jd is the flexural lever arm which for this purpose can be taken as $0.9d$, giving a required shear stress of 0.398 MPa (58 psi). According to Eq. (1), the crack width, w, must be less than 3.33 mm (0.131 in.) to transmit

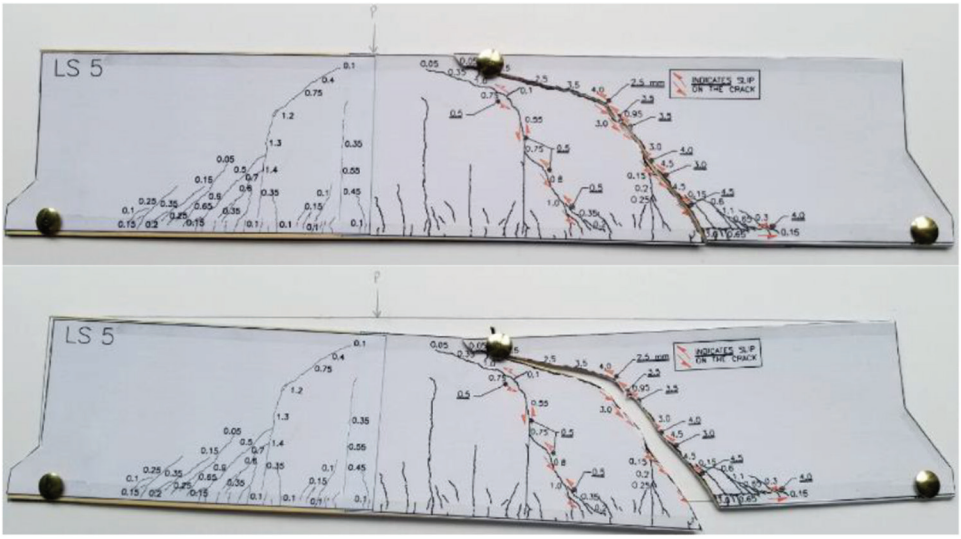

Fig. 8—Kinematics of simplified failure mechanism.

this shear stress across the crack, a width which at failure the cracks were beginning to exceed; refer to Fig. 6.

At Stage C, 37 seconds after the peak, a rapid increase in shear strain in region D2 begins, indicating that the flatter extension of the diagonal failure crack had crossed into region D2. For this flatter crack to open, kinematics requires a corresponding slip on the steeper portion of the diagonal crack; refer to Fig. 8. With the steep portion of the failure crack at 54 degrees to the horizontal while the flatter portion is at 13 degrees, the ratio of slip-to-width needs to be tan(54º – 13º) = 0.87, which is close to the measured average of 0.92. After the flatter crack formed, the rate of increase in shear strains at D2 and D3 became very similar, indicating rigid body displacement of the portion of concrete above the diagonal crack: a classic flexure-shear failure similar to that described by Joint ACI-ASCE Committee 326[17] in 1962.

At point D, 134 seconds after the peak, it was decided to decrease the displacement of the specimen to lower the load and mark and measure the crack widths and slips. Figures 5 through 8 and the associated discussion demonstrate that the flexure-shear failure of PLS4000E was a relatively slow process governed by the breakdown of aggregate interlock action as the crack widths widened and the crack faces slipped with respect to each other.

Predicted failure loads and location of failure

Equation (2), which is the ACI 318-14 basic equation for the shear strength of members not containing shear reinforcement,[6] was developed by Joint ACI-ASCE Committee 326[17] and published in 1962. The committee correctly assumed that as the flexural tensile stress in the longitudinal reinforcement increased the shear strength of the member would decrease. In a discussion, Dr. Johannes Moe suggested that this decrease in shear strength was caused by the increase in crack widths associated with higher stresses in the longitudinal reinforcement. He stated, "It now appears reasonable to assume that the amount of shear transmission across the bending cracks decreases gradually as the widths of the cracks increase."[17]

$$V_c = \left(1.9\sqrt{f'_c} + 2500\rho_w \frac{Vd}{M}\right) b_w d \quad \text{U.S. units} \qquad (2)$$

For SI units, the 1.9 is replaced by 0.16 and the 2500 is replaced by 17.2.

What was not appreciated in 1962 is that large members have their widest flexural cracks close to middepth of the member because that is where the largest crack spacing occurs. For two slabs, one twice as thick as the other, with the same strain in the flexural tension reinforcement, the thicker slab will have crack widths near middepth approximately twice as wide as those of the thinner slab. Because of their wider cracks, thicker slabs will fail at lower shear stresses, a phenomenon referred to as the size effect in shear. This size effect is predicted by the MCFT,[14] which forms the basis of the AASHTO LRFD standard[18] and the Canadian CSA A23.3-14 standard.[19] In terms of ACI format, U.S. Customary units, and clear identification of the strain effect and the size effect, an appropriate MCFT expression for V_c is[20]

$$V_c = 2\sqrt{f'_c}\frac{2.25}{(1+1500\varepsilon_x)}\frac{50}{(38+s_x)} b_w d \qquad (3)$$

where ε_x is the calculated longitudinal strain at middepth of the member; and s_x is the effective longitudinal spacing of the flexural cracks at middepth of the member. If the member has at least minimum shear reinforcement satisfying traditional spacing limits, s_x can be taken equal to 12 in. (approximately 300 mm) and the size effect is eliminated. If the member has no shear reinforcement and the maximum specified aggregate size, a_g, is at least 1 in. (25 mm), then s_x is taken as $0.75d$. For smaller maximum aggregate sizes, s_x is taken as $1.25d/(0.65 + a_g)$, which for the large test specimen is $1.25 \times 151.2/(0.65 + 0.55) = 157.5$ in. (4 m). The value of ε_x can be taken as one-half the strain in the flexural tension reinforcement where the tension force in this reinforcement is taken as $M/(0.9d) + V$.

A flexural-shear failure begins when a flexural crack become too wide to transmit the required shear stress across

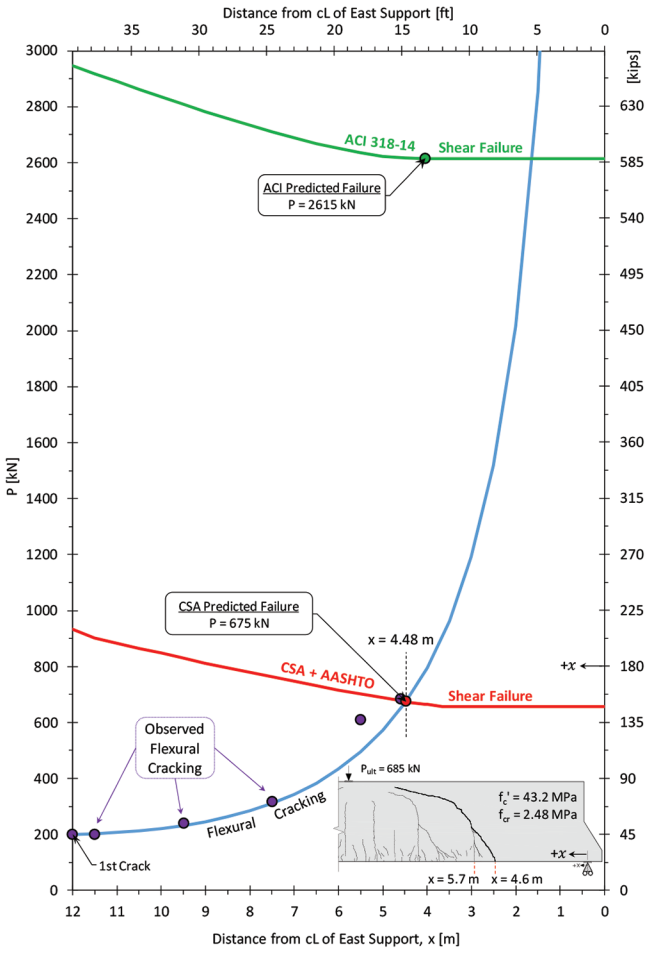

Fig. 9—Predicted and observed loads to cause flexural cracking and shear failures for east span, PLS4000E.

the crack. Figure 9 shows the values of the point load P required to cause flexural cracking at different sections along the east span of the large slab strip specimen and also shows the predicted values of P required to cause shear failure at these sections. Because of the local vertical compressive stresses caused by the point load and the support reaction, sections closer than d to the face of the support or the face of the load will not be critical in shear. The CSA and AASHTO provisions predict that the large slab strip will undergo a flexure-shear failure when the applied point load reaches 675 kN (152 kip) and a flexural crack initiates at 4.48 m (14.7 ft) from the center of the support. The 2014 ACI provisions, on the other hand, predict that the flexural-shear failure will not occur until the point load reaches 2615 kN (588 kip) with the critical section being at d from the face of the support. Thus, while the CSA and AASHTO provisions predict the point load to cause failure at 99% of the test value, the ACI 318-14 provisions predict failure at 382% of the test value.

Since completion of this paper, ACI has published the standard ACI 318-19,[21] which includes a size effect for members without stirrups. If these new provisions are applied to the experiment, the point load predicted to cause shear failure is 394 kN (88.7 kip), indicating the code is now safe, if very conservative.

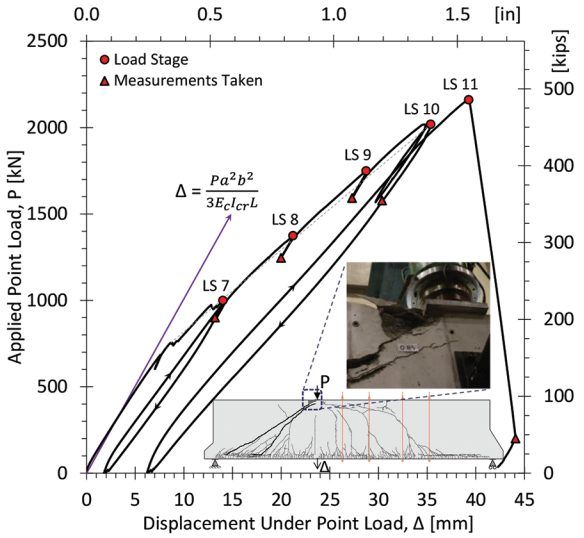

Load Stage	P, kN	P_{meas}, kN	Δ, mm	w_{max}*, mm	ε_{long}†, x 10^{-3}	ε_{vert}‡, x 10^{-3}
7	1000	900	14.0	2.5	0.79	0.64
8	1374	1246	21.2	2.5	1.10	0.99
9	1749	1592	28.7	4.0	1.42	1.08
10	2019	1578	35.4	5.5	1.68	1.14
11	2161	200	39.3	-	1.87	1.25

* Max crack width in west span
† Maximum measured longitudinal reinforcement strain
‡ Maximum measured transverse reinforcement strain

Fig. 10—Observed load-deformation response of PLS4000W.

BEHAVIOR OF WEST SPAN WITH SHEAR REINFORCEMENT

After the failed east shear span was repaired with external post-tensioned bars, the slab strip was then reloaded to investigate the response of the west shear span, PLS4000W.

Load-deformation response

Figure 10 summarizes the load-deformation response of PLS4000W. Note that the initial deflection under the point load was set to zero at the start of this second phase of loading. The initial stiffness of the already-cracked specimen closely matched that predicted by using the traditionally calculated value of I_{cr}. The pattern of cracks at failure (P = 2161 kN, [486 kip]) and the measured crack widths at 93% of the failure load are shown in Fig. 11(a). The final failure was initiated by the sudden crushing of what Mihaylov et al.[22] call the critical loading zone (CLZ), a region which in short shear spans subjected to point loads transmits a large portion of the total shear. When this zone crushed, the displacement-controlled load P reduced to just 9% of its peak value; refer to Fig. 11(b).

Note that the combination of the shorter shear span and the presence of minimum shear reinforcement in the west span increased the point load to cause failure by a factor of 3.15 and the deflection at failure by a factor of 2.87, causing an increase in the energy required to cause failure by a factor of approximately 9.

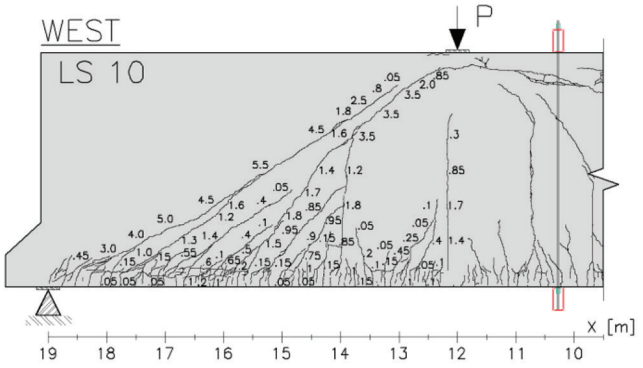

(a) Crack widths (mm) at P = 2019 kN (454 kips) 1 mm = 0.039 in.

(b) Failure at P = 2162 kN (486 kips)

Fig. 11—Crack widths near failure and pattern of cracking and crushing at failure.

Predicted failure load of PLS4000W

While PLS4000W contained a little more than the ACI-specified minimum amount of shear reinforcement, the spacing of this shear reinforcement was 2.5 times the ACI maximum specified spacing. To account for the detrimental effects of such wide spacing, the CSA code suggests that the s_x term in Eq. (3) be taken as (s – 300) mm [(s – 12) in.], which for PLS4000W is 1200 mm (47 in.).

As in the ACI Code, the shear strength of a section is taken as the sum of V_c and V_s, where V_c is given by Eq. (3) and V_s is given by Eq. (4)

$$V_s = \frac{A_v}{s} f_y 0.9d \cot\theta \quad (4)$$

The angle of inclination of the principal compressive stresses in the concrete is taken as

$$\theta = 29 \text{ degrees} + 7000\varepsilon_x \quad (5)$$

where the value of ε_x can be taken as one-half the strain in the flexural tension reinforcement when the tension force in this reinforcement is taken as $M/(0.9d) + V$.

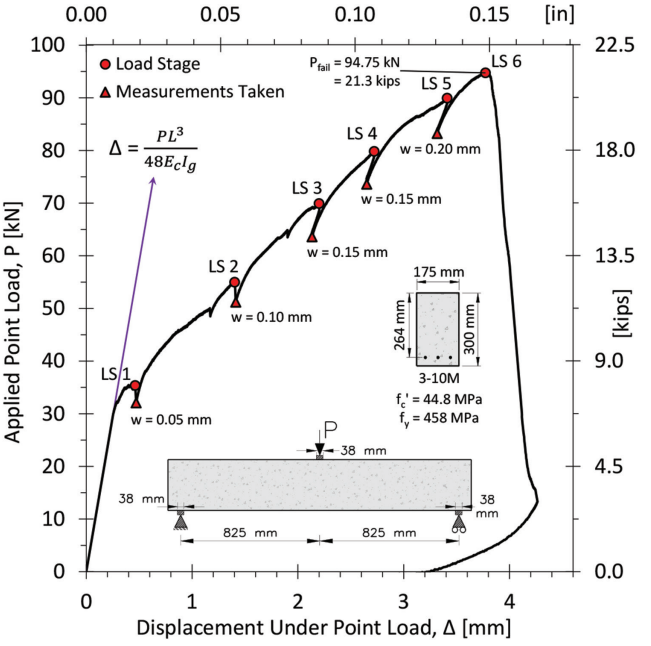

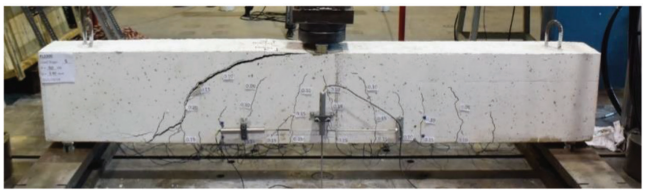

Fig. 12—Traditional size shear specimen: PLS300, load-deformation response and failure behavior.

Finally, for members with large amounts of shear reinforcement, a check needs to be made to ensure that this shear reinforcement yields before the concrete crushes.

$$V_n = V_c + V_s \le 0.22 f_c' b_w d \quad (6)$$

For short shear spans, such as PLS4000W, where the distance from the loading plate to the support plate is less than 2d, the 1962 ACI Committee 326 report[17] recommended that the critical section be taken midway along the clear shear span. Solving Eq. (3), (4), and (5) by trial and error produces a predicted shear force to cause failure of 1089 kN (245 kip) given that the self-weight shear at this location is 144 kN (32.4 kip) and the self-weight moment is 651 kN-m (480 kip ft). The experimentally observed shear force at failure was 1509 kN (339 kip), giving a test-to-predicted ratio of 1.38 by the CSA equations for sectional shear failures when applied to a member with an a/d of only 1.82.

BEHAVIOR OF TRADITIONAL-SIZED SPECIMEN

Specimen PLS300 was cast with concrete from Truck 1 and was loaded 100 days after casting, at which time the concrete cylinder strength was 44.8 MPa (6500 psi). The intent was to make a small-scale model of PLS4000E so that a direct comparison of the effect of member size on shear stress at failure could be made. Thus, both PLS300 and PLS4000E had a shear span-depth ratio a/d of 3.12, were cast with the same concrete and contained approximately the same

Table 1—Toronto size effect series

Name	d, mm	b_w, mm	f_c', MPa	a_g, mm	A_s/bd, %	$A_v f_y/b_w s$, MPa	a/d	w_{max}, mm	$\Delta/L \times 10^{-3}$	V_{exp}*, kN	V_{exp}, kN/m	v_{exp}†, MPa	V_{exp}/V_{csa}	V_{exp}/V_{aci}
BN12.5	110	300	37.2	10.0	0.909	0	3.07	0.15	5.62	40.1	134	1.215	1.17	1.20
BN25	225	300	37.2	10.0	0.889	0	3.00	0.25	2.91	73.0	243	1.081	1.12	1.07
PLS300	264	175	44.8	14.0	0.649	0	3.13	0.20	2.58	47.8	273	1.035	1.16	0.93
S-10N1	280	122	41.9	10.0	0.831	0	2.89	0.10	2.15	36.6	300	1.071	1.12	1.00
S-10H	280	122	77.3	9.5	0.831	0	2.89	0.20	1.96	37.7	309	1.104	1.09	0.80
S-10HS	280	122	77.3	9.5	1.317	0.500	2.89	2.00	4.70	66.3	543	1.941	1.09	0.99
AT-2/250B	439	252	38.5	10.0	0.904	0	2.96	0.40	1.81	114	452	1.030	1.18	1.00
AT-2/1000A	439	1002	39.0	10.0	0.909	0	2.96	0.15	1.98	476	475	1.082	1.24	1.04
AT-2/3000	440	3005	40.6	10.0	0.908	0	2.95	0.15	1.79	1310	436	0.991	1.12	0.94
BN50	450	300	37.2	10.0	0.815	0	3.00	0.25	2.00	132	440	0.978	1.19	0.97
BN100	925	300	37.2	10.0	0.757	0	2.92	0.30	1.10	192	640	0.692	1.06	0.68
BM100	925	300	47.0	10.0	0.757	0.400	2.92	2.50	3.85	342	1140	1.232	0.86	0.80
L-10N1	1400	300	38.4	9.5	0.833	0	2.89	0.55	1.05	265	883	0.631	1.09	0.61
L-10N2	1400	300	40.3	9.5	0.833	0	2.89	0.40	1.00	243	810	0.579	0.98	0.55
L-10H	1400	300	73.6	9.5	0.833	0	2.89	0.50	0.80	240	800	0.571	1.03	0.41
L-10HS	1400	300	71.2	9.5	1.333	0.500	2.89	4.00	3.35	710	2367	1.690	0.95	0.89
YB2000/0	1890	300	33.6	10.0	0.741	0	2.86	0.40	0.74	258	860	0.455	0.98	0.47
YB2000/6	1890	300	36.2	10.0	0.741	0.330	2.86	5.00	3.07	553	1843	0.975	1.01	0.73
PLS4000E	3840	250	43.2	14.0	0.656	0	3.13	0.90	0.50	393	1572	0.409	1.01	0.38
PLS4000W	3840	250	44.2	14.0	0.656	0.420	1.82	5.50	2.81	1509	6036	1.572	1.12	1.04
												Avg.	1.08	0.82
												COV	8.7%	29%

*Calculated at CSA critical section.

†Note that $v = \frac{V}{b_w \times d}$.

percentage of longitudinal, flexural tension reinforcement, $A_s/(bd) = 0.65\%$.

The observed load-deformation response of PLS300, the maximum measured crack widths at the first five load stages and the appearance of the specimen after the sudden shear failure at load stage 6 ($P = 94.8$ kN [21.3 kip]), are all shown in Fig. 12.

The maximum crack spacing at middepth for this small specimen was 210 mm (8.3 in.), 0.80d, and at 94% of failure load, the maximum crack width was 0.20 mm (0.008 in.). For PLS4000E, the maximum crack spacing at middepth was 2610 mm (103 in.), 0.68d, and at 91% of the failure load, the maximum crack width was 0.90 mm (0.035 in.). The nominal shear stress at failure for PLS300 was 149 psi (1.03 MPa), while for PLS4000E the nominal shear stress at failure was only 53 psi (0.365 MPa). Thus, as the effective depth increased by a factor of 14.5, the maximum crack spacing increased by a factor of 12.4, the crack widths near failure increased by a factor of approximately 4.5, and the shear stress to cause failure reduced by a factor of approximately 2.8.

TORONTO SIZE EFFECT SERIES

Table 1 gives the details of the 20 specimens which make up the Toronto size effect series,[23] with the slab strip specimens listed in order of increasing effective depth, d, from 110 mm (4.3 in.) to 3.84 m (12 ft 7 in.). Note that four of the specimens are made from high-strength concrete, $f_c' = 75$ MPa (10,800 psi), while the other 16 have an average concrete strength of 39.8 MPa (5800 psi) with a coefficient of variation (COV) of 9%. Fifteen of the specimens contain no shear reinforcement, while the remaining five contain approximately the ACI's specified amount of minimum shear reinforcement.

Figure 13 compares the observed shear strengths with the 2014 ACI and 2014 CSA predictions for the 15 specimens from Table 1, which have no shear reinforcement and also extends the range of depths to include that used in the Wilshire Grand mat foundation described in Fig. 1. Note that the CSA predictions closely match the experimental results as the depth increases. The vertical step in the CSA prediction occurs as the critical section transitions from near the point load to near the support with the step due to the significant self-weight shear between these locations. Because the ACI 318-14 shear provisions do not account for the size effect, the ACI predictions become more unconservative as

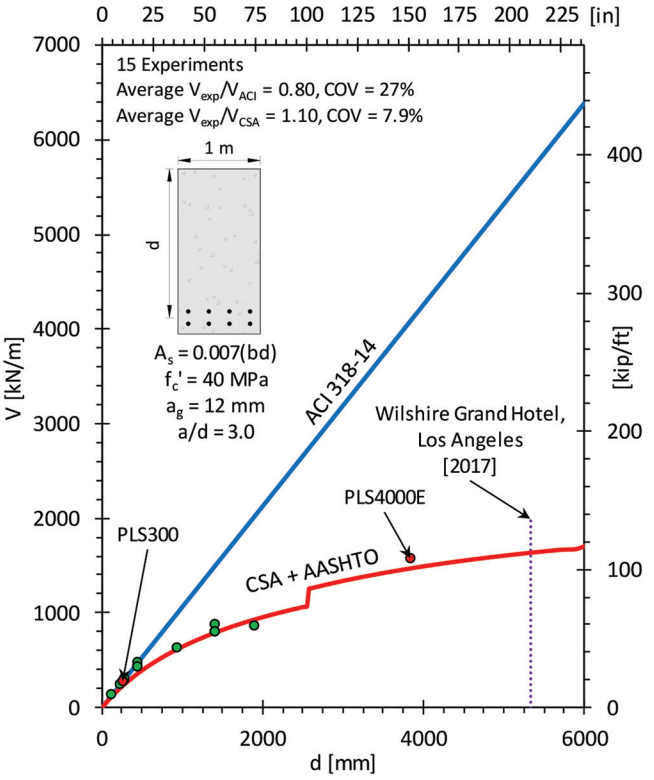

Fig. 13—Toronto size effect series, no shear reinforcement.

the depth increases. For the large depth used in the Wilshire Grand foundation, the ACI 318-14 prediction is 3.8 times larger than the CSA prediction. It should be noted, however, that the size effect in shear was taken into consideration in the design of the Wilshire Grand foundation.

Using minimum shear reinforcement in thick slabs substantially increases the shear capacity by suppressing the size effect and has the additional advantage of increasing the deformability of the member. Figure 14 shows the effect of increasing member depth on the deflection-to-span ratios at peak load (Δ/L). For members without shear reinforcement, it can be seen that the failure becomes much more brittle as the depth increases with the deflection to span ratio decreasing by a factor of more than 10 from the shallowest to deepest member. Over the same range, however, the members with minimum stirrups show a decrease in the midspan displacement at shear failure of a factor of only 1.5. Note that for members without shear reinforcement that are thicker than approximately 250 mm (10 in.), shear failures occur at a midspan deflection of less than the traditional serviceability limits. Such small deflections will make it difficult to identify members very close to a brittle shear failure.

CONCLUSIONS

Because very thick concrete slabs, such as the Wilshire Grand mat foundation, are now being built more frequently, it is important that design provisions which were developed from experiments on smaller members are updated to cover current practice. With respect to this, the following conclusions can be drawn from the experiments reported in this paper:

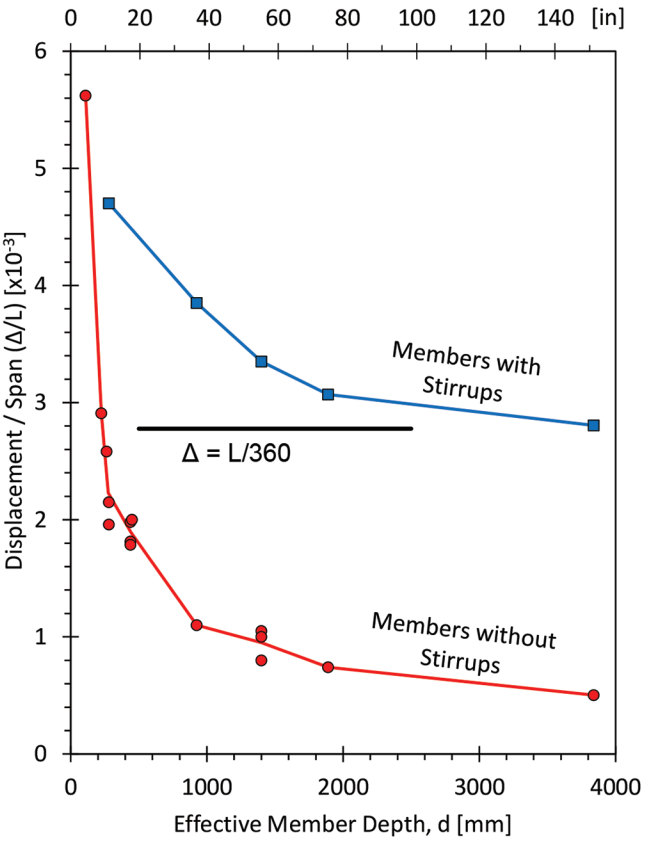

Fig. 14—Increase in deformability of members with minimum stirrups.

1. Large members without shear reinforcement fail by sliding on the critical diagonal crack when the applied shear stress exceeds the aggregate interlock capacity. In the 4000 mm (13 ft) thick test reported in this paper, a slip of 4.5 mm (0.18 in.) was observed.

2. The 2014 ACI shear provisions neglect the size effect in shear and produce very unconservative estimates of the shear strength of large members without stirrups.

3. The benefits of including at least minimum shear reinforcement in thick slabs are significantly underestimated by the 2014 ACI code. Such minimum shear reinforcement suppresses the size effect in shear.

Large members without shear reinforcement fail in shear at imperceptibly low midspan displacements, making identification of members close to a shear failure very difficult.

AUTHOR BIOS

ACI Honorary Member **Michael P. Collins** *is a Professor of structural engineering at the University of Toronto, Toronto, ON, Canada, where he has led a long-term research project aimed at developing rational but simple shear and torsion design procedures for both reinforced and prestressed concrete members. The results of this work have influenced design provisions for buildings, bridges, nuclear containment structures, and offshore concrete platforms. He has six awards from ACI.*

Phillip T. Quach *is a licensed structural engineer working at RJC Engineers in Toronto. He received his BASc and MASc with honors from the University of Toronto's Department of Civil Engineering in 2013 and 2016, respectively. He received the ACI Design Award in 2017.*

Evan C. Bentz, *FACI, is Professor and Associate Chair (undergrad) of civil engineering at the University of Toronto. He received his BASc from the University of Waterloo, Waterloo, ON, Canada, in 1994 and his PhD from the University of Toronto in 2000. He is a member of Joint ACI-ASCE*

Committee 445, Shear and Torsion, and is past Chair of ACI Committee 365, Service Life Modeling. He received the ACI Chester Paul Seiss Award in 2018 and the ACI Design Award twice.

ACKNOWLEDGMENTS

This project would not have been possible without the assistance of many experienced engineers, technicians, and research assistants. Headed Reinforcement Corporation (HRC) was kind enough to donate the headed reinforcement and the couplers while Dufferin Construction, an operating division of Holcim Canada, generously donated the large quantity of concrete. In addition, Aluma Systems supplied and erected the formwork, Amherst Group did the concrete pumping, and Ontario Cutting and Coring assisted with the demolition of the tested specimen. The enthusiasm and skill of the laboratory staff and of the research assistants made it possible to complete this complex project in the limited time available. This includes technicians R. Basset, J. MacDonald, G. Buzzeo, M. Fiss, B. Cook, and X. Sun. Finally, the long-term support of the Natural Sciences and Engineering Research Council of Canada (NSERC) is greatly appreciated.

NOTATION

A_b = area of reinforcing bar
A_s = area of longitudinal reinforcement
A_v = area of transverse reinforcement
a = shear span
a_g = maximum aggregate size
b or b_w = member width
COV = sample coefficient of variation
d = effective depth
E_c = modulus of elasticity of concrete
E_s = modulus of elasticity of steel
f_c' = concrete strength measured on test day
f_{cr} = measured flexural concrete tensile stress
f_u = measured ultimate strength of reinforcement
f_y = measured yield strength of reinforcement
h = overall member height
I_{cr} = cracked moment of inertia
I_g = gross moment of inertia
jd = flexural lever arm, taken as $0.9d$
L = span of member
M = moment at section
P = maximum applied actuator load at load stage
P_{fail} = maximum applied load to cause specimen failure
P_{meas} = load when measurements were taking during load stage
s = spacing of transverse reinforcement
s_x = crack spacing parameter with influence of aggregate size
V = shear force
V_{aci} = shear capacity as calculated by ACI 318-14 code
V_{csa} = shear capacity as calculated by CSA A23.3-14 code
V_{exp} = measured shear force
V_n = nominal shear strength
V_s = shear strength provided by shear reinforcement
v = sectional shear stress = $V/(b_w d)$
v_{ci} = interface shear stress across diagonal crack
v_{exp} = measured shear stress
w = crack width
w_{max} = maximum observed crack width
x_{crack} = location of eastern-most crack in specimen measured from center of east support
Δ = vertical displacement underneath point load
ε_c' = strain at peak concrete cylinder stress
ε_{long} = maximum measured strain in longitudinal reinforcement
ε_{sh} = steel strain at strain hardening
ε_u = steel strain at ultimate strength
ε_x = longitudinal strain at middepth of member
γ_{xy} = shear strain
θ = angle of inclination of diagonal compressive stresses to longitudinal axis of member
ρ_l or ρ_w = total percentage of longitudinal reinforcement

REFERENCES

1. Joseph, L. M., and Maranian, P. J., "Grand Performance," *Journal of Civil Engineering*, ASCE, V. 87, No. 9, Oct 2017, pp. 48-78.

2. Kani, G. N. J., "How Safe are Our Large Reinforced Concrete Beams?" *ACI Structural Journal*, V. 64, No. 3, Mar. 1967, pp. 128-141.

3. Bažant, Z. P., and Kim, J.-K., "Size Effect in Shear Failure of Longitudinal Reinforced Beams," *ACI Journal Proceedings*, V. 81, pp. 456-468, and Disc. V. 82, 1984, pp. 579-583.

4. Shioya, T.; Iguro, M.; Nojiri, Y.; Akiyama, H.; and Okada, T., "Shear Strength of Large Reinforced Concrete Beams," *Fracture Mechanics: Applications to Concrete*, SP-118, V. C. Li and Z. P. Bažant, eds., American Concrete Institute, Farmington Hills, MI, 1989, pp. 259-279.

5. Collins, M. P., and Kuchma, D., "How Safe Are Our Large, Lightly Reinforced Concrete Beams, Slabs, and Footings?" *ACI Structural Journal*, V. 96, No. 4, July-Aug. 1999, pp. 482-490.

6. ACI Committee 318, "Building Code Requirements for Structural Concrete (ACI 318-14) and Commentary (ACI 318R-14)," American Concrete Institute, Farmington Hills, MI, 2014, 519 pp.

7. Xie, L.; Bentz, E. C.; and Collins, M. P., "Influence of Axial Stress on Shear Response of Reinforced Concrete Elements," *ACI Structural Journal*, V. 108, No. 6, Nov.-Dec. 2011, pp. 745-754.

8. Collins, M. P.; Bentz, E. C.; Quach, P. T.; and Proestos, G. T., "The Challenge of Predicting the Shear Strength of Very Thick Slabs," *Concrete International*, V. 37, No. 11, Nov. 2015, pp. 29-37. (CI)

9. Reineck, K.-H.; Bentz, E.; Fitik, B.; Kuchma, D. A.; and Bayrak, O., "ACI-DAfStb Databases for Shear Tests on Slender Reinforced Concrete Beams with Stirrups," *ACI Structural Journal*, V. 111, No. 5, Sept.-Oct. 2014, pp. 1147-1156. doi: 10.14359/51686819

10. Quach, P. T., *Understanding and Safely Predicting the Shear Response of Large-Scale Reinforced Concrete Structures*, University of Toronto, Toronto, ON, Canada, 2016, 305 pp.

11. Bentz, E. C., "Empirical Modeling of Cracking in Reinforced Concrete," *ACI Structural Journal*, V. 116, No. 3, May 2019, pp. 233-242. doi: 10.14359/51714476

12. Calvi, P. M.; Bentz, E. C.; and Collins, M. P., "Reversed Cyclic Experiments on Shear Stress Transfer across Cracks in Reinforced Concrete Elements," *ACI Structural Journal*, V. 113, No. 4, July-Aug. 2016, pp. 851-859. doi: 10.14359/51688926

13. Walraven, J. C., "Fundamental Analysis of Aggregate Interlock," *Journal of the Structural Division*, ASCE, V. 107, No. 11, 1981, pp. 2245-2270.

14. Vecchio, F. J., and Collins, M. P., "The Modified Compression-Field Theory for Reinforced Concrete Elements Subjected to Shear," *ACI Structural Journal*, V. 83, No. 2, Mar.-Apr. 1986, pp. 219-231.

15. Bhide, S. B., and Collins, M. B., "Influence of Axial Tension on the Shear Capacity of Reinforced Concrete Members," *ACI Structural Journal*, V. 86, No. 5, Sept.-Oct. 1989, pp. 570-581.

16. Sherwood, E. G.; Bentz, E. C.; and Collins, M. P., "Effect of Aggregate Size on Beam-Shear Strength of Thick Slabs," *ACI Structural Journal*, V. 104, No. 2, Mar.-Apr. 2007, pp. 180-190.

17. Joint ACI-ASCE Committee 326, "Shear and Diagonal Tension," *ACI Journal Proceedings*, V. 59, No. 1, 2, and 3, Jan., Feb., and Mar., 1962, pp. 1-30, 277-334, and 352-396 and Disc. and Clos., Oct. 1962, pp. 1323-1349.

18. AASHTO, "LRFD Bridge Design Specifications and Commentary," sixth edition, American Association of State Highway Transportation Officials, Washington, DC, 2012, 1264 pp.

19. CSA A23.3-14, "Design of Concrete Structures," Canadian Standards Association, Mississauga, ON, Canada, 2014, 291 pp.

20. Bentz, E. C., and Collins, M. P., "Updating the ACI Shear Design Provisions," *Concrete International*, V. 39, No. 9, Sept. 2017, pp. 33-38.

21. ACI Committee 318, "Building Code Requirements for Structural Concrete (ACI 318-19) and Commentary (ACI 318R-19)," American Concrete Institute, Farmington Hills, MI, 2019, 624 pp.

22. Mihaylov, B. I.; Bentz, E. C.; and Collins, M. P., "Two-Parameter Kinematic Theory for Shear Behavior of Deep Beams," *ACI Structural Journal*, V. 110, No. 3, May-June 2013, pp. 447-456.

23. Bentz, E. C., and Collins, M. P., "The Toronto Size Effect Series," *Shear in Structural Concrete*, SP-328, American Concrete Institute, Farmington Hills, MI, 2018, 12 pp.

APPENDIX

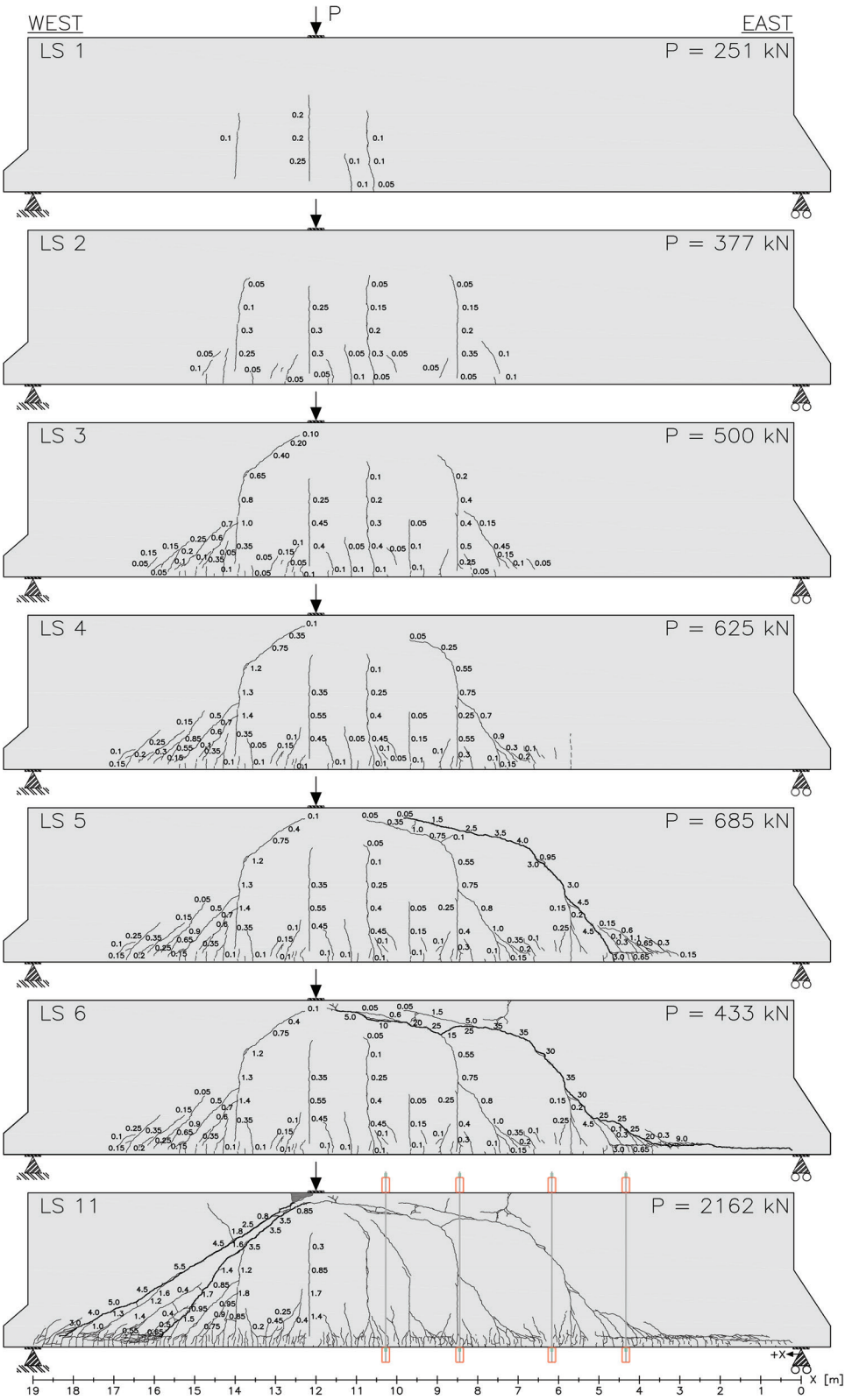

Fig. A1—Crack diagrams at all load stages.